Toward an Operational Dynamical Model of Lateral Manual Interception Behavior

Danial Borooghani, Remy Casanova, Frank T.J.M. Zaal, Reinoud J Bootsma

Motor Control, (Ahead of Print)
https://doi.org/10.1123/mc.2024-0036
First Published Online: Nov. 20, 2024

Human Kinetics
ARTICLE

Toward an Operational Dynamical Model of Lateral Manual Interception Behavior

Danial Borooghani,[1] Remy Casanova,[1] Frank T.J.M. Zaal,[2] and Reinoud J. Bootsma[1]

[1]Institut des Sciences du Mouvement, Aix-Marseille Université, CNRS, Marseille, France; [2]Department of Human Movement Sciences, University Medical Center Groningen, Groningen, The Netherlands

We develop a dynamics-based model of discrete movement for lateral manual interception capable of generating movements with realistic kinematics. For the present purposes, we focus on the situation of to-be-intercepted targets moving at constant speed along rectilinear trajectories oriented orthogonally with respect to the interception axis. The proposed phenomenological model is designed to capture the time evolution of empirically observed hand movements along the interception axis under different conditions of target arrival location and target speed-induced time pressure. Pattern formation dynamics combine a Duffing stiffness function, allowing for creating a fixed-point attractor at the perceived location of the target arrival on the interception axis, with a hybrid Rayleigh plus Van der Pol damping function. After parametrizing the model for required movement direction (left/right), amplitude, and duration, it adequately reproduces the (variations in) empirically observed kinematics with a single set of four coefficients for all conditions considered. The model is also demonstrated to inherently incorporate speed–accuracy trade-off characteristics.

Keywords: stability, emerging, motion analysis, behavioral dynamics, kinematics, kinetics

The study of interceptive actions has been at the heart of movement science for more than half a century, dating back to the seminal work of Whiting on perception and action in ball catching (Sharp & Whiting, 1974; Whiting, 1968, 1969; Whiting

Borooghani https://orcid.org/0000-0002-8537-5586
Casanova https://orcid.org/0000-0002-7101-8043
Zaal https://orcid.org/0000-0003-2697-3612
Bootsma (reinoud.bootsma@univ-amu.fr) is corresponding author, https://orcid.org/0000-0002-3719-7586

et al., 1970; Whiting & Sharp, 1974). Interceptive actions are indeed paradigmatic examples of our behavioral interaction with dynamic elements of the environment. However, notwithstanding the wealth of work on the prime examples of catching and hitting, to date, there is still no operational model available capable of realistically capturing how we manage even the basic requirement of any interceptive action of getting to the right place at the right time. This basic requirement is arguably most purely incorporated in the task of lateral (i.e., direction-constrained) interception, in which the agent's action is restricted to movement along a fixed interception axis, which is the focus of the present contribution.

The first attempt at modeling lateral manual interception behavior was grounded in the idea that the hand movement would be guided by a (perceived and continuously updated) required velocity, defined as the ratio of the current lateral distance between hand and target over the time remaining until the target reaches the interception axis (Peper et al., 1994; also see Dessing et al., 2002). In this model, the hand velocity is continuously driven toward the currently required velocity, with the latter being modulated by a faster-than-linear activation function (cf. Bullock & Grossberg, 1988). Inclusion of such an activation function was necessary to ensure a smooth initial rise in hand velocity and sufficiently rapid integration of differences between current and required hand velocity in subsequent phases. Although this first-order dynamics type of model allowed for capturing—at least the qualitative aspects of—kinematic phenomena observed in interception behavior (as reported in Montagne et al., 1999; Peper et al., 1994), its initial structure and development over time (Dessing et al., 2004, 2005, 2009) have revealed several limitations. First, inclusion of an activation function is in fact problematic, given this element's predominant role in the shaping of the resulting movement. Second, model extensions have given rise to an inflation of hypothesized system components, thereby dissolving the parsimony of the initial idea.

Models based in autonomous second-order dynamics, on the other hand, allow for the emergence of trajectory formation without recourse to arbitrary, yet influential supplementary components such as an activation function, nor for that matter to any global optimization criterion as often used in computational modeling of discrete movements (e.g., Hasan, 1986; Hogan, 1984; Kawato et al., 1990; Nelson, 1983). Such autonomous second-order dynamics models take the general form (Beek & Beek, 1988; Jordan & Smith, 1987)

$$\ddot{x} + g(x) + f(x,\dot{x})\dot{x} = 0, \tag{1}$$

where x, $\dot{x}$, and $\ddot{x}$ are the position, velocity, and acceleration, respectively, of the task-defined end effector considered (here the hand). In addition to the linear x and $\dot{x}$ terms, first-step expansions of the g and f functions yield the conservative Duffing term $g(x) = x^3$ and nonconservative Rayleigh $f(x,\dot{x})\dot{x} = (\dot{x}^2)\dot{x}$ and Van der Pol $f(x,\dot{x})\dot{x} = (x^2)\dot{x}$ terms. Combinations of these standard terms have been used in modeling end-effector kinematics of rhythmical movement in unconstrained and paced continuous movement tasks (Beek et al., 1996; Beek, Schmidt, et al., 1995; Haken et al., 1985; Kadar et al., 1993; Kay et al., 1987, 1991), as well as in continuous goal-directed actions such as juggling (Beek & Beek, 1988) and reciprocal aiming (Bongers et al., 2009; Mottet & Bootsma, 1999). Given the sustained, rhythmical nature of the behaviors addressed, these studies naturally focused on the dynamics of limit cycle behavior. However, as pointed out by

Schöner (1990, also see Gonzalez & Piro, 1987), nonlinear dynamical systems typically have more than one regime, including point attractors as required for modeling discrete movement behavior, which is the behavior observed in the lateral manual interception task that is the focus of the present contribution. Compared with rhythmical movements, to date, the pattern formation dynamics underlying discrete movement behavior have not been studied as extensively, with emphasis having mostly been focused on (continuous) shifts of a single equilibrium position (Bizzi et al., 1982; Feldman, 1986; Hogan, 1984; McIntyre & Bizzi, 1993; Ostry & Feldman, 2003; Polit & Bizzi, 1978; Schweighofer et al., 1998).

For the present purposes, we therefore build on two theoretical contributions addressing pattern formation dynamics for discrete movement. Schöner (1990) proposed that discrete movements could be generated by a dynamical system with two stable point attractors, located at the initial and to-be-reached positions. In his model, the intention to move, instantiated as "behavioral information" (BI), is expressed as an additional component in the equation of motion, allowing for driving the system from the fixed-point regime into a limit cycle regime when BI is turned on. Turning BI off, about halfway through the cycle, brings the system back into the stable fixed-point regime, leading it to relax toward the final point. The Jirsa and Kelso (2005) excitator model also uses BI, in this case to push a bistable attractor point system over a local flow-segregating separatrix into the attraction basin of the final point attractor. It is important to notice that in both proposals this BI only serves to push the system into a desired regime or state; it is not prescriptive of the particular aspects of the movement to be made (Schöner, 1990). In the following, we prefer to refer this contribution to the pattern dynamics as "behavioral seed" (BS) to reserve the term information for perceptual quantities.

In developing his initial proposal in the field of robotics, Schöner subsequently integrated task requirements in the form of (perceived) constraints on behavior, allowing for scaling the movement's amplitude and duration (Oubbati & Schöner, 2013; Schöner, 1994a, 1994b; Schöner et al., 1995; Schöner & Santos, 2001). By including spatial and temporal constraints into the model, it became capable of generating movements arriving at a perceptually defined place after a perceptually-defined time, as in discrete interception movements. We note, however, that the above-cited contributions, using generic (normal form) state equations, were developed to demonstrate the principles of a nonlinear dynamics account for time and space constrained discrete movements but did not attempt to capture empirically observed end-effector kinematics. As our goal is precisely to model such empirically observed end-effector kinematics, we drew inspiration from this theoretical work but took the somewhat different route of starting from a second-order dynamic of the general form provided by Equation 1 already explored in earlier data-driven modeling studies of rhythmic behavior (e.g., Beek et al., 1996; Beek, Schmidt et al., 1995; Kay et al., 1987, 1991; Mottet & Bootsma, 1999). We note that, using such an approach, Zaal et al. (1999) modeled discrete reaching toward targets that were either stationary or moving (away from the initial hand position) along the reaching movement axis. They thus included a particular type of lateral manual interception, requiring the hand to catch up with the moving target. Following Schöner's (1990) suggestion of a (partial) limit cycle implication, Zaal et al.'s (1999) Duffing–Rayleigh limit cycle model adequately captured experimentally observed relations among movement amplitude, movement time,

and peak velocity. This study, however, did not address the transition from limit cycle to the (subsequent) fixed-point regime and therefore remains incomplete. It is also worth highlighting that, as the to-be-reached target moved along the hand movement axis, the task did not directly constrain either where or when the target was to be intercepted, as is the case for the type of data that we want to model.

Given that to date there is no complete model capable of generating realistic lateral manual interception movements, we proceed by first identifying what we want our model to be able to capture, as this defines its basic characteristics. To independently vary where and when the target is to be intercepted, the task must have target trajectories that cross the interception axis. Studies using such target trajectories have revealed a variety of influences of target trajectory characteristics on the kinematics of the interceptive actions produced (e.g., Arzamarski et al., 2007; Dessing et al., 2005; Ledouit et al., 2013; Michaels et al., 2006; Montagne et al., 1999, 2000; Peper et al., 1994), including effects of distance to be covered, time pressure, and target trajectory orientation with respect to the interception axis. In most of the above cited empirical studies, targets could cross the interception axis at different distances on the left and on the right of the initial hand position. Our model thus needs to be able to generate both leftward and rightward movements.

Data Set Used for Modeling

For the present modeling purposes, we therefore needed a data set of lateral manual interceptive movements collected for participants being confronted with targets that could reach the interception axis at different locations, on the left and on the right side of the initial end-effector position, after different target motion durations. The data collected in the study of lateral manual interception reported by Ledouit et al. (2013) fitted these requirements. Briefly, in this study, participants moved a handheld stylus (represented on screen by a 0.1-cm wide white line cursor) along a horizontal interception axis situated near the bottom of a digitizing tablet's screen to intercept virtual targets (hereafter referred to as balls, represented by a 0.8-cm diameter white circle,) moving from top to bottom across the black-background screen toward the interception axis at one of two constant speeds (20 or 32 cm/s), leading to ball motion durations of 1.6 and 1.0 s. From Ledouit et al.'s (2013) data set, we retained the orthogonal ball trajectories (no sideward ball motion component) that crossed the interception axis at lateral distances of −14, −7, +7, and +14 cm from the initial stylus position. Figure 1 presents the ensemble-average kinematic profiles of the recorded lateral interception movements, which the present contribution aims to model.

As can be seen from Figure 1, the distance to be covered and time available both affected the movement kinematics, notably in terms of the timing and magnitude of peak velocity reached and the overall shape of the velocity–time curve.

Model Structure

The model developed for generating these different movements was built in the following way. With balls arriving both left and right of the starting position, we modified Schöner's (1990) and Jirsa and Kelso's (2005) lead of using a Duffing function to create stable equilibrium points located at the starting position and at

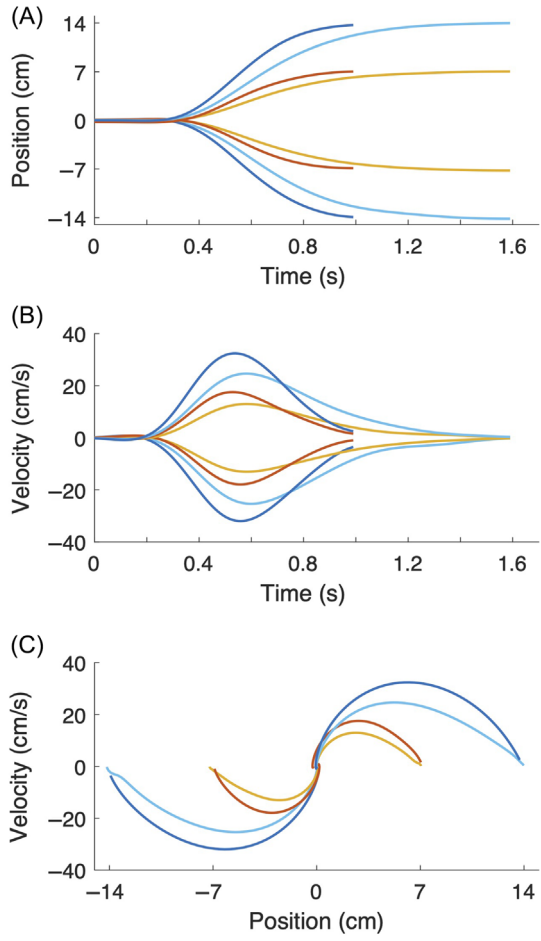

Figure 1 — Ensemble averages of empirically observed hand trajectories from Ledouit et al.'s (2013) data set for interception of uniformly moving balls following trajectories perpendicular to the interception axis, arriving at distances of −14, −7, +7, and +14 cm from the hand starting position after ball flight times of 1.6 and 1.0 s. (A) Position as a function of time, (B) velocity as a function of time, and (C) phase portraits (velocity as a function of position). (Color figure online).

the goal position, with BS pushing the hand to move the system into the attraction basin of the goal position. We note that, in both of these approaches, the origin of the reference frame used is located halfway between the stable equilibrium points that define the starting and goal positions. Movement from the starting position is thus typically unilateral.

To circumvent this, we parametrized the Duffing function to switch from a monostable regime with the equilibrium point located at the starting position (here coinciding with the origin of the reference frame) to a bistable stable regime with

equilibrium points located at the required distance to the left and right of the starting position. As a result of this switch, the starting position becomes an unstable equilibrium point. A (relatively small) signed BS contribution is used to push the system in the required direction, to the left or to the right. We note that this left–right feature of our model is also needed if we want to include reversal movements (interception on the right characterized by an initial leftward movement component, or vice versa, as reported by Montagne et al., 1999, under particular target trajectory conditions) in future model applications.

Let us begin by clarifying what the above implies for the parametrization of the conservative Duffing terms:

$$\ddot{x} + kx + ax^3 = 0. \tag{1a}$$

Positioning an equilibrium point (where $\ddot{x} = \dot{x} = 0$) at the location on the interception axis where the ball arrives (i.e., goal location x_g) implies that $k = -ax_g{}^2$. Substituting for k in Equation 1a results in

$$\ddot{x} - ax_g{}^2x + ax^3 = 0, \tag{1b}$$

which is rewritten as

$$\ddot{x} + ax(x^2 - x_g{}^2) = 0. \tag{1c}$$

With x_g initially set to 0, the starting position $x = 0$ is the equilibrium point of a monostable regime ($\ddot{x} + ax^3 = 0$). Switching x_g to a non-zero value sets up two stable equilibrium points at $\pm x_g$, while destabilizing the $x = 0$ starting position (see exemplary phase-space vector field representation in Figure 2). In the present framework, the intention to move, underlying the switch in x_g, is triggered

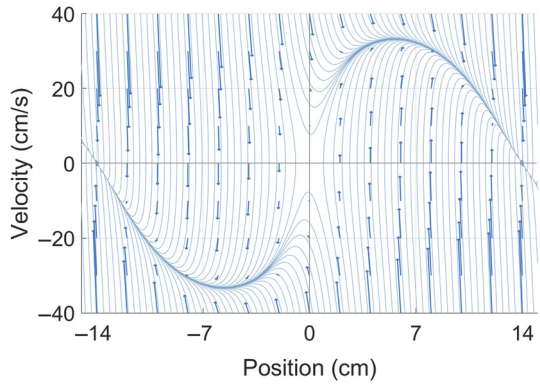

Figure 2 — Exemplary vector field representation of the phase space of the bistable attractor point regime of the model. The origin (0, 0) is a repellor, whereas in this example (−14, 0) and (+14, 0) are attractors. Pushing the system rightward from its (0, 0) initial location leads it to follow the stabilized trajectory to (+14, 0); pushing the system leftward from its (0, 0) initial location leads it to follow the stabilized trajectory to (−14, 0). Note that the areas of interest are the first and third quadrants.

by the ball motion information coming to the fore with respect to its future arrival position on the interception axis. The signed BS, set equal to x_g, pushes the system in the desired direction, away from the (unstable) starting position, so that

$$\ddot{x} + ax(x^2 - {x_g}^2) + f\mathrm{BS} = 0. \quad (2)$$

To dampen the system during movement and allow for the variations in the shape of the velocity profile observed in the empirical data, we included both nonconservative Rayleigh and Van der Pol terms. Such hybrid Rayleigh and Van der Pol damping is quite common in dynamical modeling of upper limb movements (Kay et al., 1987; Mottet & Bootsma, 1999; Schmidt et al., 2015).

In the presence of these two nonlinear terms (both only dissipating energy as the system remains in a fixed-point regime), inclusion of a linear damping term ($b\dot{x}$) is no longer required nor necessarily appropriate in the current framework as it may lead to redundancy in the model. We come back to this point in the "Discussion" section. The final model structure thus becomes

$$\ddot{x} + ax(x^2 - {x_g}^2) + d\dot{x}^3 + ex^2\dot{x} + f\mathrm{BS} = 0. \quad (3)$$

Figure 3 highlights the effects of the Rayleigh and Van der Pol terms on the velocity profile of movements generated with this model structure.

Scaling the Model to the Data

We recall that our data set contains interception movements with different amplitudes (ball arrival positions at 7 and 14 cm, to the left and to the right of

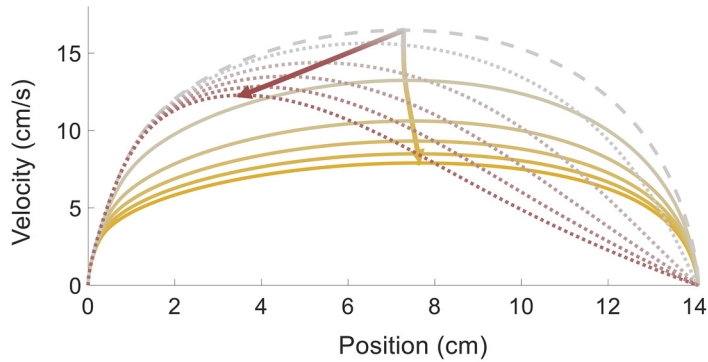

Figure 3 — Phase portraits of (rightward) movements generated by the dynamical system captured by Equation 3, demonstrating the influences of Rayleigh and Van der Pol damping terms on the kinematic shapes. For all simulations, coefficient a was set to 0.5 and x_g to 14, while coefficients of the Rayleigh term (d) and the Van der Pol term (e) were independently varied. The top dashed gray curve corresponds to $d = e = 0.1$. Dotted gray to red variations reflect effects of increasing e (0.1, 0.2, 0.4, 0.6, 0.8, and 1.0) for $d = 0.1$. Gray to orange variations reflect effects of increasing d (0.1, 0.2, 0.4, 0.6, 0.8, and 1.0) for $e = 0.1$. Arrows track changes in the location of peak velocity. (Color figure online).

the starting position) and different temporal constraints (balls reaching the interception location in 1.6 and 1.0 s). The model must therefore be scaled to these constraints. Following Peper et al. (1994), we assume that, at the moment of onset of the movement, information is available specifying both future ball arrival position on the interception axis (with the goal location, i.e., specified ball arrival position denoted as x_b) and time until the ball reaches this position (with specified ball flight time denoted as T_f).

Scaling the model to the data is therefore to be done by modulation of the coefficients of model terms by x_b and T_f. The magnitude of the Duffing coefficient a influences the duration of the movement as larger a's are associated with larger initial accelerations and hence shorter movement durations. The perceived time constraint T_f may thus be incorporated by modulating coefficient a by T_f. Given the condition-dependent kinematic features of the observed interceptive movements (Figure 1), further modulating influences of space–time constraints x_b and T_f on model parameters are also expected.

Fitting the Model to the Data

For the present purposes, we assumed that information about the future ball arrival position on the interception axis and ball flight time became available after 150 ms of ball motion across the screen, as empirical hand acceleration tended to rapidly increase thereafter. For each ball motion condition, we therefore switched the initial goal location $x_g = 0$ to the perceived ball arrival location $x_g = x_b$ and simultaneously turned BS on at that time. BS was subsequently turned off 300 ms later. With BS thus being activated at 150 ms after trial onset and deactivated 300 ms later, BS is in fact a function of time, hereafter denoted as BS(t).

In fitting the model to the data, we concurrently explored the presence of systematic modulatory influences of movement amplitude $|x_b|$ and ball flight time T_f on the model's coefficients by including both, each with potential powers of +1, 0, and −1. As a result, coefficient modulation by these two ball trajectory-specific constraints could only be proportional, null, or inverse proportional in nature. This choice was made for reasons of parsimony.

The final form of the model fitted to the data was

$$\ddot{x} + \mathrm{M}_1 a' x(x^2 - {x_b}^2) + \mathrm{M}_2 d' \dot{x}^3 + \mathrm{M}_3 e' x^2 \dot{x} + \mathrm{M}_4 f' \mathrm{BS}(t) = 0, \tag{4}$$

where each M_i is a modulation parameter defined as $\mathrm{M}_i = |x_b|^{m_i} \cdot {T_f}^{n_i}$, with m, $n = -1$, 0 or +1.

Fitting was performed using a nonlinear gradient-based optimization method (fmincon MATLAB function). To prevent the algorithm from getting stuck in local position error minima, we performed multiple fits, exploring the effects of varying initial settings and lower and upper boundaries of the different parameters.

This procedure yielded a final result of the form

$$\ddot{x} + \frac{1}{|x_b| T_f} a' x(x^2 - {x_b}^2) + d' \dot{x}^3 + \frac{1}{|x_b|} e' x^2 \dot{x} + \frac{1}{T_f} f' \mathrm{BS}(t) = 0, \tag{5}$$

with values of $a' = 15.3223$, $d' = 0.0164$, $e' = 5.3504$, and $f' = -1.2601$, for a total Root Mean Square Deviation (RMSD) = 2.60 cm, corresponding to an average RMSD of 0.32 cm for each individual trajectory.

As expected, time available to reach the interception location (T_f) exerted an inverse proportional modulatory influence on the parameter of the Duffing term, such that shorter ball flight times gave rise to higher initial accelerations. A similar (inverse proportional) influence on the Duffing term was observed for the required amplitude of movement ($|x_b|$). This latter result can be understood as ensuring that, at the early stages of movement (i.e., for small values of x) the resulting acceleration $\ddot{x} = -\frac{1}{|x_b|}ax(x^2 - {x_b}^2) = -\frac{1}{|x_b|}ax^3 + ax|x_b|$ is scaled to (the absolute value of) x_b rather than to ${x_b}^2$, thereby avoiding acceleration rising too vigorously for larger distances to be covered.

The optimization procedure revealed that Rayleigh and Van der Pol damping terms indeed played complementary roles. With larger movement distances requiring less damping, the Van der Pol term was inverse proportionally modulated by $|x_b|$, whereas no such modulating was required for the Rayleigh term. Analogously to the above interpretation of the inverse proportional $|x_b|$ modulation of the Duffing term, its modulatory effect on the Van der Pol term can be understood as following from the need to avoid too vigorous ($x^2\dot{x}$-induced) damping at larger distances from the starting position.

Finally, optimization indicated that the BS(t), providing a temporary push in the required direction of magnitude x_b, was inverse proportionally modulated by the time constraint T_f. Thus, BS(t) in fact became proportional to x_b/T_f, which corresponds to the (perceptually specified) initial required velocity, as defined by Peper et al. (1994).

Figure 4 presents the trajectories generated by this parametrized model for each of the four ball arrival positions under each of the two ball flight durations.

Discussion

As can be seen from Figure 4, parametrized with the required movement direction (sign of x_b in BS), movement amplitude $|x_b|$, and movement duration T_f, the minimal four-coefficient model proved capable of generating interceptive movements exhibiting the pertinent kinematic characteristics of the empirically observed movements under the different conditions examined. These characteristics are most adequately defined via the velocity profiles and can be characterized in terms of (a) the magnitude of peak velocity, (b) the timing of peak velocity, (c) the overall shape of the velocity profile, and (d) the velocity at the time of interception. The model reproduced the observed larger magnitude of peak velocity for the larger movement amplitude and, at each movement amplitude, the larger magnitude of peak velocity for the shorter T_f. It reproduced the observed shift in the moment of occurrence of peak velocity, which was reached somewhat later for the longer T_f for both movement amplitudes. It reproduced the observed elongation of the right-side tail of the velocity profile (i.e., of the deceleration phase) for the longer T_f for both movement amplitudes. And, finally, it reproduced the observed velocity at the time of interception, with, for both movement amplitudes, this velocity falling to zero for the longer T_f but not fully so for the shorter T_f.

Of course, the model did not perfectly reproduce the empirically observed movements. A first reason for this is that the observed leftward and rightward

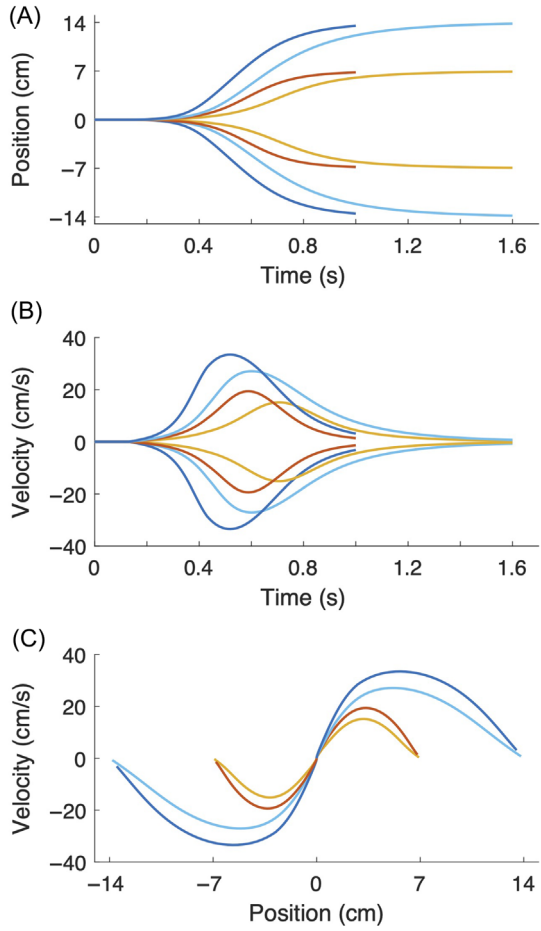

Figure 4 — Final model (Equation 5) simulation results for interceptive movements of balls following trajectories perpendicular to the interception axis, arriving at distances of −14, −7, +7, and +14 cm for the hand starting position after ball flight times of 1.6 and 1.0 s, with coefficient settings $a' = 15.3223$, $d' = 0.0164$, $e' = 5.3504$, and $f' = -1.2601$. (A) Position as a function of time, (B) velocity as a function of time, and (C) phase portraits (velocity as a function of position). (Color figure online).

interception movements were not fully symmetrical, as can be seen from Figure 1. Quantitatively, this symmetrical discrepancy amounted to an RMSD of 0.80 cm. We note that this amounts to some 30% of the overall (2.60 cm) RMSD of the model fit, indicating the model indeed captured the common kinematic characteristics quite well. We did not seek to adapt the model to be able to account for the left–right asymmetry observed in the selected data set, notably because for now we want it to remain as simple and general as possible. For the same reasons, we also did not include between-condition variations in the moment of onset of movement,

which could explain the model's somewhat slower-than-observed rise in velocity for the shorter movement amplitudes. This could be mitigated via a later onset of BS in the simulations of these particular conditions. The finding that the magnitude of BS, providing an initial push in the required direction, was in fact best set proportional to the ratio of x_b over T_f is interesting as it thereby creates a soft connection between the current model and Peper et al.'s (1994) initial required velocity model.

As mentioned earlier, our choice to not include a linear damping term in the to-be-fitted model structure was based on the potential redundancy (in terms of fitting) of incorporating three damping terms. Indeed, fitting the model (Equation 4) with an additional linear damping term may inappropriately return a negative coefficient for this term, indicating energy injection rather than dissipation (see Mottet & Bootsma, 1999, p. 243, for a discussion of similar fitting problems). For the record, we note that fitting the model with combinations of linear and either Rayleigh or Van der Pol damping did not allow for capturing the empirically observed kinematic characteristics and their variations under the four $x_b \times T_f$ combinations to a sufficiently satisfactory extent.

The operational dynamical model for lateral manual interception behavior developed in the present contribution seeks to capture the pattern formation principles at work in such spatiotemporally constrained discrete movements. As such, to paraphrase Beek, Peper, et al. (1995) it is a mathematical, phenomenological model that does not seek to provide an account of the observed phenomena in terms of their underlying causes. Rather, it allows for capturing—and further exploring—the regularities in the time evolution of the action system under different environmental conditions, here captured by the space–time constraints on the interceptive action. In this regard it is important to bear in mind that the goal of the participants in the Ledouit et al. (2013) study of lateral manual interception—from which the data modeled here were extracted—was to simply intercept the ball, making it closer to catching (e.g., Dessing et al., 2005; Michaels et al., 2006; Montagne et al., 1999; Peper et al., 1994) than to hitting. (e.g., Bootsma & Van Wieringen, 1990; Smeets & Brenner, 1995; Tresilian & Lonergan, 2002; Tresilian & Houseman, 2005). Catching and hitting tasks indeed differ in several aspects, perhaps most clearly brought out by the velocity profiles of the (hand) movements deployed. Our catching task is characterized by an initial rise and subsequent fall in the movement velocity over time, which can even approach zero at the moment of interception for longer ball flight durations (see Figure 1). Hitting tasks, on the other hand, are typically characterized by a movement velocity that continuously increases over time, with peak velocity being reached close to the moment of contact. As the movement behaviors are thus quite different, whether hitting movements can be captured by a model structure of the type developed in the present contribution for now remains an open question.

In the present contribution, we moved from proof of concept (Schöner, 1990; Jirsa & Kelso, 2005) to the production of realistic movement patterns for direction-constrained manual interception. Although the model developed was demonstrated to adequately capture ensemble-average movement patterns under different space and time constraints, motor performance is typically also characterized by some degree of variability, both in the movement pattern and in the outcome. In order

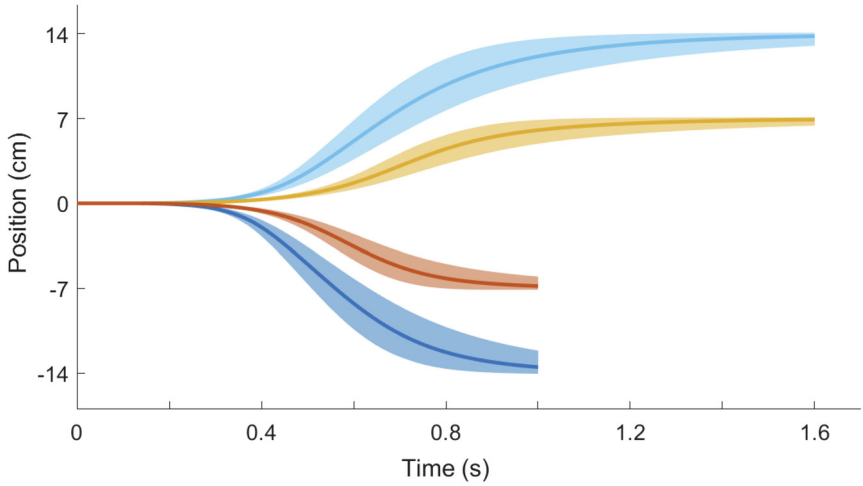

Figure 5 — Results of 500 runs of the parameterized model (Equation 5), with each run producing movement trajectories (thin lines, together creating surfaces) for all four combinations of movement duration and amplitude (for reasons of readability, rightward for 1.6-s duration and leftward for 1.0-s durations). Coefficients a', d', and e' vary over runs as a result of multiplying each with a random number between 0.7 and 1.3, thereby adding 30% noise to the coefficients. The thick lines in each panel represented the model without noise. Note that the number of trajectories above and below the thick (no-noise) model trajectory are approximately equal.

to tentatively explore the model's potential in accommodating such variability, we probed the effect of range-delimited random variations in model coefficients over repeated simulations of the four combinations of ball flight time (1.0 and 1.6 s) and ball arrival position (7 and 14 cm). Figure 5 presents an example of 500 movement trajectories thus generated (using Equation 5) for each condition with a 30% between-trial noise on coefficients a', d', and e'. Visual inspection of these families of movement trajectories revealed the typical (rising and falling) pattern of between-trial variability as a function of time for goal-directed movements (Darling & Cooke, 1987; Darling et al., 1988; Hansen et al., 2008).

Taking this analysis one step further, we also examined the outcome variability. The original data from Ledouit et al. (2013) revealed a pattern of spatial endpoint variability (captured by spatial variable error at the moment of ball arrival) corresponding to the well-known speed–accuracy trade-off (see Plamondon & Alimi, 1997, for a review): spatial variable error was largest for interceptive actions requiring the highest movement speed (i.e., 14-cm distance to be covered in 1.0 s) and smallest for interceptive actions requiring the lowest movement speed (i.e., 7-cm distance to be covered in 1.6 s), with the other two intermediate movement speed conditions producing intermediate variable error magnitudes. The exemplary model simulations shown in Figure 5 in fact reproduced this pattern: spatial variable errors calculated on the original data and on the model simulations revealed close to identical patterns, $r(4) = .993$, $p = .007$;

$R^2 = .985$. The model dynamics thus inherently incorporate the speed–accuracy trade-off. Future work within this research program will address the general pertinence of the model by testing it on different lateral manual interception data sets. We also intend to use the model to explore its potential in capturing two particularly intriguing findings in lateral interception: the angle-of-approach effect and, relatedly, the movement-reversal effect. The former effect resides in the presence of systematic differences in hand movement kinematics when intercepting rectilinearly moving targets arriving at the same interception position after the same flight duration while coming from different starting positions (Arzamarski et al., 2007; Ledouit et al., 2013; Montagne et al., 1999; Peper et al., 1994). The latter effect, of movement starting toward the left before intercepting the ball on the right, or vice versa, occurs under particular ball trajectory conditions when participants initiate their interceptive movement early on after movement onset (Montagne et al., 1999). For the present purposes, from the Ledouit et al.'s (2013) data set, we only retained the ball trajectories that were orthogonally oriented with respect to the interception axis. However, this data set also contains ball trajectories with different angles of approach to the same interception location and can therefore be used to explore the model's capability (e.g., by having the goal location evolve over time) of reproducing the angle-of-approach effect. It could, in a similar way, also be capable of generating reversal movements.

Acknowledgment

This project received funding from the European Union's Horizon 2020 research and innovation program under the Marie Skłodowska-Curie grant agreement no. 956,003.

References

Arzamarski, R., Harrison, S.J., Hajnal, A., & Michaels, C.F. (2007). Lateral ball interception: Hand movements during linear ball trajectories. *Experimental Brain Research, 177*(3), 312–323. https://doi.org/10.1007/s00221-006-0671-8

Beek, P.J., & Beek, W.J. (1988). Tools for constructing dynamical models of rhythmic movement. *Human Movement Science, 7*(2–4), 301–342. https://doi.org/10.1016/0167-9457(88)90015-2

Beek, P.J., Peper, C.E., & Stegeman, D.F. (1995). Dynamical models of movement coordination. *Human Movement Science, 14*(4–5), 573–608. https://doi.org/10.1016/0167-9457(95)00028-5

Beek, P.J., Rikkert, W.E.I., & Van Wieringen, P.C.W. (1996). Limit cycle properties of rhythmic forearm movements. *Journal of Experimental Psychology: Human Perception and Performance, 22*(5), 1077–1093. https://doi.org/10.1037/0096-1523.22.5.1077

Beek, P.J., Schmidt, R.C., Morris, A.W., Sim, M.-Y., & Turvey, M.T. (1995). Linear and nonlinear stiffness and friction in biological rhythmic movements. *Biological Cybernetics, 73*(6), 499–507. https://doi.org/10.1007/BF00199542

Bizzi, E., Accornero, N., Chapple, W., & Hogan, N. (1982). Arm trajectory formation in monkeys. *Experimental Brain Research, 46*(1), 139–143. http://dx.doi.org/10.1007/BF00238107

Bongers, R.M., Fernandez, L., & Bootsma, R.J. (2009). Linear and logarithmic speed–accuracy trade-offs in reciprocal aiming result from task-specific parameterization of an

invariant underlying dynamics. *Journal of Experimental Psychology: Human Perception and Performance, 35*(5), 1443–1457. https://doi.org/10.1037/a0015783

Bootsma, R.J., & van Wieringen, P.C.W. (1990). Timing an attacking forehand drive in table tennis. *Journal of Experimental Psychology: Human Perception and Performance, 16*(1), 21–29. https://doi.org/10.1037//0096-1523.16.1.21

Bullock, D., & Grossberg, S. (1988). Neural dynamics of planned arm movements: Emergent invariants and speed–accuracy properties during trajectory formation. *Psychological Review, 95*(1), 49–90. https://doi.org/10.1037/0033-295X.95.1.49

Darling, W.G., Cole, K.J., & Abbs, J.H. (1988). Kinematic variability of grasp movements as a function of practice and movement speed. *Experimental Brain Research, 73*(2), 225–235. https://doi.org/10.1007/BF00248215

Darling, W.G., & Cooke, J.D. (1987). Changes in the variability of movement trajectories with practice. *Journal of Motor Behavior, 19*(3), 291–309. https://doi.org/10.1080/00222895.1987.10735414

Dessing, J.C., Beek, P.J., Caljouw, S.R., & Peper, C.L.E. (2004). A dynamical neural network for hitting an approaching object. *Biological Cybernetics, 91*(6), 377–387. https://doi.org/10.1007/s00422-004-0520-4

Dessing, J.C., Bullock, D., Peper, C.E., & Beek, P.J. (2002). Prospective control of manual interceptive actions: Comparative simulations of extant and new model constructs. *Neural Networks, 15*(2), 163–179. https://doi.org/10.1016/S0893-6080(01)00136-8

Dessing, J.C., Oostwoud Wijdenes, L., Peper, C.L.E., & Beek, P.J. (2009). Adaptations of lateral hand movements to early and late visual occlusion in catching. *Experimental Brain Research, 192*(4), 669–682. https://doi.org/10.1007/s00221-008-1588-1

Dessing, J.C., Peper, C.E., Bullock, D., & Beek, P.J. (2005). How position, velocity, and temporal information combine in the prospective control of catching: Data and model. *Journal of Cognitive Neuroscience, 17*(4), 668–686. https://doi.org/10.1162/0898929053467604

Feldman, A.G. (1986). Once more on the equilibrium-point hypothesis (λ model) for motor control. *Journal of Motor Behavior, 18*(1), 17–54. https://doi.org/10.1080/00222895.1986.10735369

Gonzalez, D.L., & Piro, O. (1987). Global bifurcations and phase portrait of an analytically solvable nonlinear oscillator: Relaxation oscillations and saddle-node collisions. *Physical Review A, 36*(9), 4402–4410. https://doi.org/10.1103/PhysRevA.36.4402

Haken, H., Kelso, J.A.S., & Bunz, H. (1985). A theoretical model of phase transitions in human hand movements. *Biological Cybernetics, 51*(5), 347–356. https://doi.org/10.1007/BF00336922

Hansen, S., Elliott, D., & Khan, M.A. (2008). Quantifying the variability of three-dimensional aiming movements using ellipsoids. *Motor Control, 12*(3), 241–251. https://doi.org/10.1123/mcj.12.3.241

Hasan, Z. (1986). Optimized movement trajectories and joint stiffness in unperturbed, inertially loaded movements. *Biological Cybernetics, 53*(6), 373–382. https://doi.org/10.1007/BF00318203

Hogan, N. (1984). An organizing principle for a class of voluntary movements. *Journal of Neuroscience, 4*(11), 2745–2754. http://www.jneurosci.org/content/4/11/2745.short

Jirsa, V.K., & Kelso, J.A.S. (2005). The excitator as a minimal model for the coordination dynamics of discrete and rhythmic movement generation. *Journal of Motor Behavior, 37*(1), 35–51. https://doi.org/10.3200/JMBR.37.1.35-51

Jordan, D.W., & Smith, P. (1987). *Nonlinear ordinary differential equations*. Clarendon Press.

Kadar, E.E., Schmidt, R.C., & Turvey, M.T. (1993). Constants underlying frequency changes in biological rhythmic movements. *Biological Cybernetics, 68*(5), 421–430. https://doi.org/10.1007/BF00198774

Kawato, M., Maeda, Y., Uno, Y., & Suzuki, R. (1990). Trajectory formation of arm movement by cascade neural network model based on minimum torque-change criterion. *Biological Cybernetics, 62*(4), 275–288. https://doi.org/10.1007/BF00201442

Kay, B.A., Kelso, J.A., Saltzman, E.L., & Schöner, G. (1987). Space–time behavior of single and bimanual rhythmical movements: Data and limit cycle model. *Journal of Experimental Psychology: Human Perception and Performance, 13*(2), 178–192. https://doi.org/10.1037/0096-1523.13.2.178

Kay, B.A., Saltzman, E.L., & Kelso, J.A. (1991). Steady-state and perturbed rhythmical movements: A dynamical analysis. *Journal of Experimental Psychology: Human Perception and Performance, 17*(1), 183–197. https://doi.org/10.1037/0096-1523.17.1.183

Ledouit, S., Casanova, R., Zaal, F.T.J.M., & Bootsma, R.J. (2013). Prospective control in catching: The persistent angle-of-approach effect in lateral interception. *PLoS One, 8*(11), Article e80827. https://doi.org/10.1371/journal.pone.0080827

McIntyre, J., & Bizzi, E. (1993). Servo hypotheses for the biological control of movement. *Journal of Motor Behavior, 25*(3), 193–202. https://doi.org/10.1080/00222895.1993.9942049

Michaels, C.F., Jacobs, D.M., & Bongers, R.M. (2006). Lateral interception II: Predicting hand movements. *Journal of Experimental Psychology: Human Perception and Performance, 32*(2), 459–472. https://doi.org/10.1037/0096-1523.32.2.459

Montagne, G., Fraisse, F., Ripoll, H., & Laurent, M. (2000). Perception-action coupling in an interceptive task: First-order time-to-contact as an input variable. *Human Movement Science, 19*(1), 59–72. https://doi.org/10.1016/S0167-9457(00)00005-1

Montagne, G., Laurent, M., Durey, A., & Bootsma, R.J. (1999). Movement reversals in ball catching. *Experimental Brain Research, 129*(1), 87–92. https://doi.org/10.1007/s002210050939

Mottet, D., & Bootsma, R.J. (1999). The dynamics of goal-directed rhythmical aiming. *Biological Cybernetics, 80*(4), 235–245. https://doi.org/10.1007/s004220050521

Nelson, W.L. (1983). Physical principles for economies of skilled movements. *Biological Cybernetics, 46*(2), 135–147. https://doi.org/10.1007/BF00339982

Ostry, D.J., & Feldman, A.G. (2003). A critical evaluation of the force control hypothesis in motor control. *Experimental Brain Research, 153*(3), 275–288. https://doi.org/10.1007/s00221-003-1624-0

Oubbati, F., & Schöner, G. (2013). Autonomous timed movement based on attractor dynamics in a ball hitting task. In *Proceedings of the 5th International Conference on agents and artificial intelligence, February 15–18, 2013, Barcelona, Spain* (pp. 304–311). https://doi.org/10.5220/0004324003040311

Peper, L., Bootsma, R.J., Mestre, D.R., & Bakker, F.C. (1994). Catching balls: How to get the hand to the right place at the right time. *Journal of Experimental Psychology: Human Perception and Performance, 20*(3), 591–612. https://doi.org/10.1037/0096-1523.20.3.591

Plamondon, R., & Alimi, A.M. (1997). Speed/accuracy trade-offs in target-directed movements. *Behavioral and Brain Sciences, 20*, 279–249. https://doi.org/10.1017/S0140525X97001441

Polit, A., & Bizzi, E. (1978). Processes controlling arm movements in monkeys. *Science, 201*(4362), 1235–1237. https://doi.org/10.1126/science.99813

Schmidt, R.C., Corey, D., Fitzpatrick, P., & Riley, M.A. (2015). The oscillatory basis of Fitts' law. In B.G. Bardy, R.J. Bootsma, & Y. Guiard (Eds.), *Studies in perception and action III: Eighth international conference on perception and action, July 9–14, 1995, Marseille, France* (1st ed., pp. 95–98). Routledge. https://doi.org/10.4324/9781315789361

Schöner, G. (1990). A dynamic theory of coordination of discrete movement. *Biological Cybernetics, 63*(4), 257–270. https://doi.org/10.1007/BF00203449

Schöner, G. (1994a). 17—From interlimb coordination to trajectory formation: Common dynamical principles. In S.P. Swinnen, H. Heuer, J. Massion, & P. Casaer (Eds.), *Interlimb coordination: Neural, dynamical, and cognitive constraints* (pp. 339–368). Academic Press. https://doi.org/10.1016/B978-0-12-679270-6.50022-X

Schöner, G. (1994b). Dynamic theory of action-perception patterns: The time-before-contact paradigm. *Human Movement Science, 13*(3–4), 415–439. https://doi.org/10.1016/0167-9457(94)90048-5

Schöner, G., Dose, M., & Engels, C. (1995). Dynamics of behavior: Theory and applications for autonomous robot architectures. *Robotics and Autonomous Systems, 16*(2–4), 213–245. https://doi.org/10.1016/0921-8890(95)00049-6

Schöner, G., & Santos, C. (2001). Control of movement time and sequential action through attractor dynamics: A simulation study demonstrating object interception and coordination. In *SIRS 2001 Proceedings of the 9th International symposium on intelligent robotic systems, July 18–20, 2001, Toulouse, France* (pp. 15–24). https://repositorium.sdum.uminho.pt/bitstream/1822/4327/1/paper_25jan2001.pdf

Schweighofer, N., Arbib, M.A., & Kawato, M. (1998). Role of the cerebellum in reaching movements in humans. I. Distributed inverse dynamics control. *European Journal of Neuroscience, 10*(1), 86–94. https://doi.org/10.1046/j.1460-9568.1998.00006.x

Sharp, R.H., & Whiting, H.T.A. (1974). Exposure and occluded duration effects in a ball-catching skill. *Journal of Motor Behavior, 6*(3), 139–147. https://doi.org/10.1080/00222895.1974.10734990

Smeets, J.B., & Brenner, E. (1995). Perception and action are based on the same visual information: Distinction between position and velocity. *Journal of Experimental Psychology: Human Perception and Performance, 21*(1), 19–31. https://doi.org/10.1037/0096-1523.21.1.19

Tresilian, J., & Lonergan, A. (2002). Intercepting a moving target: Effects of temporal precision constraints and movement amplitude. *Experimental Brain Research, 142*(2), 193–207. https://doi.org/10.1007/s00221-001-0920-9

Tresilian, J.R., & Houseman, J.H. (2005). Systematic variation in performance of an interceptive action with changes in the temporal constraints. *The Quarterly Journal of Experimental Psychology Section A, 58*(3), 447–466. https://doi.org/10.1080/02724980343000954

Whiting, H.T.A. (1968). Training in a continuous ball throwing and catching task. *Ergonomics, 11*(4), 375–382. https://doi.org/10.1080/00140136808930985

Whiting, H.T.A. (1969). *Acquiring ball skills: A psychological interpretation*. Bell.

Whiting, H.T.A., Gill, E.B., & Stephenson, J.M. (1970). Critical time intervals for taking in flight information in a ball-catching task. *Ergonomics, 13*(2), 265–272. https://doi.org/10.1080/00140137008931141

Whiting, H.T.A., & Sharp, R.H. (1974). Visual occlusion factors in a discrete ball-catching task. *Journal of Motor Behavior, 6*(1), 11–16. https://doi.org/10.1080/00222895.1974.10734974

Zaal, F.T.J.M., Bootsma, R.J., & van Wieringen, P.C.W. (1999). Dynamics of reaching for stationary and moving objects: Data and model. *Journal of Experimental Psychology: Human Perception and Performance, 25*(1), 149–161. https://doi.org/10.1037/0096-1523.25.1.149